Symmetry-protected bound states in the continuum supported by all-dielectric metasurfaces

Shiyu Li,[1] Chaobiao Zhou,[2,*] Tingting Liu,[3] and Shuyuan Xiao[4,5]

[1]*Wuhan National Laboratory for Optoelectronics, Huazhong University of Science and Technology, Wuhan 430074, China*
[2]*College of Mechanical and Electronic Engineering, Guizhou Minzu University, Guiyang 550025, China*
[3]*School of Physics and Electronics Information, Hubei University of Education, Wuhan 430205, China*
[4]*Institute for Advanced Study, Nanchang University, Nanchang 330031, China*
[5]*Jiangxi Key Laboratory for Microscale Interdisciplinary Study, Nanchang University, Nanchang 330031, China*

(Received 9 August 2019; revised manuscript received 28 October 2019; published 2 December 2019)

Symmetry-protected bound states in the continuum (BICs) are nonradiative states with infinite lifetime and perfect confinement of energy even though lying in the radiation continuum due to the symmetry incompatibility. Herein, we study the symmetry-protected BIC supported by metasurfaces composed of silicon nanodisks. Through adding or removing parts of the nanodisks from the edge, a sharp Fano resonance emerges and demonstrates the excitation of quasi-BIC. Their Q factors exhibit the same dependence on the asymmetry degree with these two opposite operations. Furthermore, from both qualitative and quantitative perspectives, analysis on far-field contributions from multipole moments along different directions combining with near-field distributions explains the evolution from BIC to quasi-BIC. The dominant contributor to the quasi-BIC is illustrated to be the electric quadrupole in the x-y plane. Finally, the topological charge carried by the BIC is calculated to be -1, demonstrating the topological characteristics of our design. Such metasurfaces are robust in nanofabrication. Our results may provide a route for resonators with better performance applied in sensing, switching, nonlinear optics, and so on.

DOI: 10.1103/PhysRevA.100.063803

I. INTRODUCTION

Enhancing light-matter interactions, which is significant for improving performances of devices, can be realized by confining light into subwavelength scale. Bound states in the continuum (BICs), distinct from the conventional bound states whose frequencies are outside the continuum spectrum, lie inside the continuum while remaining perfectly localized without radiation [1,2]. They were first proposed in quantum systems [3] and then developed to photonics due to their perfect confinement of energy and robust existence [4–15].

BICs can be classified into different categories based on the mechanisms of the vanishing coupling between eigenmodes of structures and the free space. The first kind is the symmetry-protected BIC existing at the Γ point of the reciprocal space based on the symmetry incompatibility between the bound state and the continuum. In a system with reflection or rotational symmetries, bound states and the continuum may belong to different symmetry classes and thus have the coupling forbidden when the symmetry is preserved [4–8]. Another so-called accidental BIC, in contrast with the symmetry-protected BIC, emerges from the destructive interference of several leaky waves at the off-Γ point through tuning the parameters of the system continuously, resulting in an accidental vanishing coupling to the radiation continuum [9–14]. While a true optical BIC is a mathematical concept that can only be realized in ideal lossless infinite structures [4,11]. In practice, BIC-inspired states with large field enhancement inside the structures and finite lifetime, the so-called quasi-BICs, are free from these limitations and have been realized in photonics crystal slabs [9,16], gratings [12], coupled optical waveguides [17], and metasurfaces and metamaterials [4–6,8,18–20]. Applications have been developed in lasing [21,22], optical sensing [23], nonlinear optics [24–28], and so on.

Most of the nanostructures used to excite these quasi-BICs with high Q factors are composite structures, such as asymmetric pairs of tilted nanobars [4,29–31], split rings [32–34], and asymmetric nanorods [35–37], which have more challenges in fabricating deep subwavelength gaps and suffer from extra scattering losses from the near-field coupled structures. Other nanostructures like notched cubes [38,39] have many sharp corners, making it difficult to be accurately fabricated through lithographic techniques, which degrades the performance of the resonators [40]. Besides, nanodisks with small broken nanoholes [25,41], another investigated structure, have difficulties in maintaining the depths of nanoholes and heights of nanodisks the same under one nanofabrication process. Therefore, nanostructures with improved fabrication tolerance and a simpler manufacturing process are needed to realize quasi-BIC resonators with better performance.

In our work, a metasurface composed of silicon nanodisks is proposed to investigate the symmetry-protected BIC. By slightly breaking the in-plane symmetry of the structures through adding or removing a part from the edge of nanodisks, quasi-BICs with Fano lineshapes are observed in the transmission, whose Q factors exhibit the same inverse quadratic dependence on asymmetry degrees with these two opposite operations. To go deeply further, the transformation from BIC

*cbzhou@gzmu.edu.cn

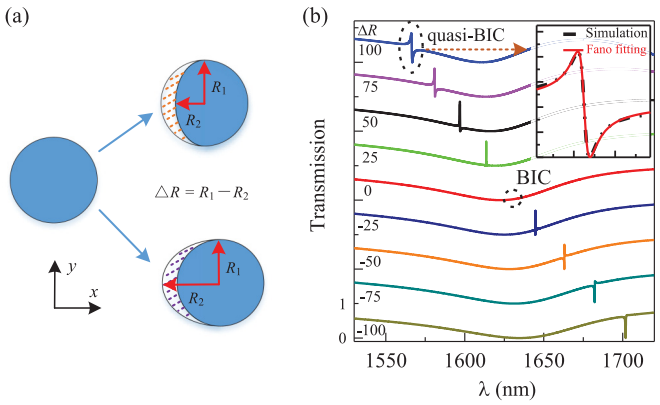

FIG. 1. (a) Geometry of a symmetric Si nanodisk and two asymmetric Si nanodisks after removing (top) or adding (bottom) a part of the disk from the left edge. There are also SiO_2 substrates under the nanodisks, which are omitted for simplicity. (b) Evolution of the transmission spectra vs the ΔR.

to quasi-BIC is analyzed in detail through calculating the far-field radiations from multipole moments along different directions and near-field distributions. These qualitative and quantitative demonstrations point out the dominant role of electric quadrupole components in the excitation of quasi-BIC. The topological nature of the BIC is also analyzed with the topological charge calculated to be -1. Our work provides a broad and deep insight into the properties of the symmetry-protected BIC supported by a simpler metasurface and may benefit the design and optimization of metasurfaces with strong light confinement.

II. THE GEOMETRIC STRUCTURE AND BIC CHARACTERISTICS

A perturbation that breaks the in-plane inversion symmetry $(x, y) - (-x, -y)$ of a structure can transform a symmetry-protected BIC into a quasi-BIC with high Q factor [4,5]. Through adding or removing a part of the structure from the edge of a highly symmetric nanodisk belonging to the symmetry group C_{4v} as shown in Fig. 1(a), a structure with in-plane asymmetry is designed to build the radiation channel between a nonradiative bound state and the free space continuum. An array of 240-nm-tall Si nanodisks with a lattice constant of 1050 nm lies on a SiO_2 substrate. The radius of the symmetric nanodisk is marked by $R_1 = 400$ nm and the length from the center to the left edge of the disk after perturbation is marked by R_2, with the asymmetry level decided by $\Delta R = R_1 - R_2$. The difference between R_1 and R_2 perturbs the in-plane symmetry of the structure, degenerating the higher order group C_{4v} to lower order group C_s, and leads to the access of leaky quasi-BIC states from true BIC states [5]. Finite-difference time-domain simulations are employed to analyze the optical properties of metasurfaces. A y-polarized plane wave is normally incident on metasurfaces. The periodical boundary conditions are set in the x and y directions and perfectly matched layers are set in the z direction. The dielectric constants of Si and SiO_2 are extracted from the Palik handbook [42]. The calculated transmission with varying ΔR is illustrated in Fig. 1(b). As ΔR decreases, corresponding to removing a smaller part from the nanodisk, the resonance becomes sharper and finally vanishes when the nanodisk is symmetric ($\Delta R = 0$). While further decreasing ΔR, which means adding a larger part to the nanodisk, the resonance grows wider again. That vanished resonance at around 1630 nm when $\Delta R = 0$, which means no leaky energy from the bound state to the free space, demonstrates the existence of a BIC state. Along with the broken symmetry of the nanodisk, obvious asymmetric Fano resonances are produced, demonstrating the emergence of a quasi-BIC. These Fano resonances originate from the interference between discrete bound states supported by nanodisks and the free space continuum [5,11]. The resonance curve can be fitted by the Fano formula [25,43,44],

$$T_{\text{Fano}}(\omega) = \left| a_1 + ja_2 + \frac{b}{\omega - \omega_0 + j\gamma} \right|^2, \tag{1}$$

as shown in the inset of Fig. 1(b), where a_1, a_2, and b are constant real numbers, ω_0 is the central resonant frequency, and γ is the overall damping rate of the resonance. The radiative Q factor Q_{rad} is determined by $Q_{\text{rad}} = \omega_0/2\gamma$.

The explanation about the relationship between BIC and quasi-BIC is depicted in Fig. 2(a). The resonant state $|\varphi\rangle$ with finite Q factor, noted as quasi-BIC, can be considered as an unperturbed, nonradiative bound state $|\varphi_0\rangle$ supported by the structure, namely BIC, interacting with the radiation continuum and finally leaks out. The influence of this interaction is specifically described by $|\varphi_1\rangle = \hat{V}|\varphi_0\rangle$, where $\hat{V}$ is the perturbation operator responsible for energy shift and coupling to the free space [11,45]. The symmetry of this $|\varphi_1\rangle$ state matches with that of a free space polarization, and thus compensates the symmetry mismatch between the BIC and outgoing wave, leading to the radiation of quasi-BIC. In our design, the BIC $|\varphi_0\rangle$ supported by the square periodical array of symmetric Si nanodisks belongs to point symmetry group C_{4v}, which can be denoted by B type based on the irreducible representation. This B-type mode is nondegenerate in the C_{4v} group, uncoupled to external radiation and possessed of infinite lifetime under normal incidence due to the symmetry mismatch [5,46,47]. Its mode profile, corresponding to the z component of the magnetic field H_z for the TE mode, is shown by color in Fig. 2(a). When the symmetry of the structure is perturbed by a removing or adding operation, the perturbation operator $\hat{V}$ will interact with the unperturbed state $|\varphi_0\rangle$ and produces $|\varphi_1\rangle$ with a net magnetic polarization along the x axis [green arrow in Fig. 2(a)], sharing the same symmetry with y-polarized light defined by the electric field. Therefore, as a combination of states $|\varphi_0\rangle$ and $|\varphi_1\rangle$, the quasi-BIC $|\varphi\rangle$ can radiate to free space with y-polarized excitation.

Further quantitative analysis is carried out on the radiation properties of this metasurface with different asymmetry levels. The resonant state $|\varphi\rangle$ can be associated with a complex frequency $\omega = \omega_0 - i\gamma$, where ω_0 and γ are the central resonant frequency and overall damping rate of the resonance, respectively. Because the lattice constant of the metasurface is less than the working wavelength in the substrate, the only radiation channel to the continuum is 0th-order diffraction [4,5]. Considering the up-down symmetry of the resonant state and applying the Lippmann-Schwinger equation and perturbation

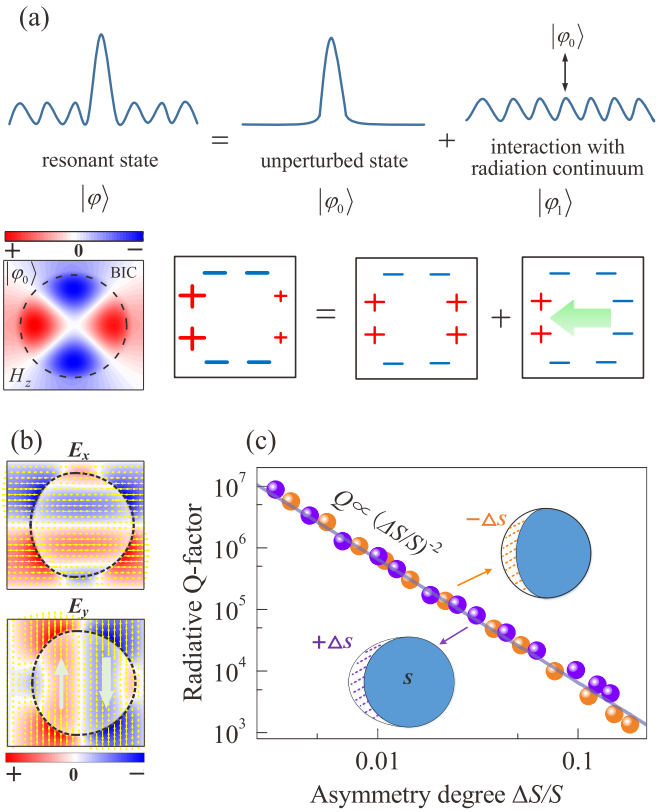

FIG. 2. (a) A scheme describing the relationship between quasi-BIC and BIC (top). The H_z profile of the unperturbed BIC (bottom, left) and a scheme decomposing the quasi-BIC into an unperturbed proportion and a perturbed proportion (bottom, right), with the colors and signs depicting the symmetries of the modes. The size of the signs represents the strength of the fields. The green arrow shows the net polarization. (b) Calculated electric fields and their directions (yellow arrows) in the x-y plane for E_x and E_y components, respectively. (c) Log-log plot of radiative Q factors as a function of the asymmetric degree $\Delta S/S$ for removing case (orange balls) and adding case (purple balls). The blue line shows the inverse quadratic dependence of $\Delta S/S$.

theory [4,48], the damping rate γ can be expressed as

$$\gamma = \frac{\omega_0^2}{4Ac}\sum_{i=x,y}\left\{\int d\vec{r}[\varepsilon(\omega_0,\vec{r})-1]E_i(\vec{r})e^{ik_0 z}\right\}^2, \quad (2)$$

where A is the surface area of a unit cell, E_i is the x or y component of the electric field in the far field of the resonant state, the integration calculates the sum electric field of the resonant state between the boundaries lying in the far field enclosing the structures. Expanding the function $e^{ik_0 z}$ into the Taylor series, there is [4]

$$\gamma = \frac{k_0^2 c}{4A}\left[\left(p_x - \frac{m_y}{c} + \frac{ik_0}{6}Q_{zx}\right)^2 + \left(p_y + \frac{m_x}{c} + \frac{ik_0}{6}Q_{yz}\right)^2\right], \quad (3)$$

where p_α, m_α, $Q_{\alpha\beta}$ $(\alpha,\beta = x,y,z)$ are the components of electric dipole, magnetic dipole, and electric quadrupole moments in the irreducible representations, respectively; k_0 is the incident wave vector in the free space. The two terms in the square bracket represent the contributions of E_x and E_y, respectively. Other higher-order multipoles are negligible due to the satisfaction of $hk_0 < 1$, where h is the height of the disk [49]. In our design, after the removing or adding behavior, the mirror transformation symmetry along the y axis is broken. Thus, E_x and E_y are classified as odd and even, respectively, as verified in Fig. 2(b). The yellow arrows in the E_x profile of Fig. 2(b) represent the directions of E_x, where the integration equals 0 due to the antisymmetric (odd) distribution. m_x and Q_{yz} equal 0 since no circular electric field and net charge exist in the y-z plane, considering the up-down symmetry $E_y(-z) = E_y(z)$. As marked with gray arrows in the E_y profile of Fig. 2(b), p_y can be understood as the uncompensated dipole moments with opposite directions supported by the two halves of the nanodisk with respect to the y axis, namely satisfying $p_y = \pm\frac{2\Delta S}{S}p_0$, where ΔS is the area of the removing or adding part, S is the area of the symmetric nanodisk, and p_0 is the electric dipole moment in the right half of the nanodisk. Using $\Delta S/S$ to describe the asymmetry degree, then the radiative Q factor $Q_{\rm rad} = \omega_0/2\gamma$ of the resonant state $|\varphi\rangle$ can be expressed as

$$Q_{\rm rad} = \frac{A}{2k_0}|p_0|^{-2}\left(\frac{\Delta S}{S}\right)^{-2}. \quad (4)$$

Figure 2(c) shows the calculated Q factors of the metasurfaces at different asymmetry degrees in both adding and removing cases, exhibiting the same inverse quadratic trend as described in Eq. (4). A more interesting phenomenon is that, through adding and removing operations, different metasurfaces with resonant wavelengths lying at two sides of the BIC position can have nearly the same Q factors when their asymmetry degrees are equivalent. That is because p_0 remains the same for the two opposite operations attributed to the unchanged right half of the nanodisk.

Next, we decompose the far-field radiation of BIC and quasi-BIC into contributions of different multipole components under the Cartesian coordinate to further discuss their characteristics. The multipole moments can be obtained based on current density $\vec{j}$ [50–52],

$$\vec{P} = \frac{1}{i\omega}\int \vec{j}d^3r, \quad (5)$$

$$\vec{M} = \frac{1}{2c}\int (\vec{r}\times\vec{j})d^3r, \quad (6)$$

$$\vec{T} = \frac{1}{10c}\int [(\vec{r}\cdot\vec{j})\vec{r} - 2r^2\vec{j}]d^3r, \quad (7)$$

$$Q^{(e)}_{\alpha\beta} = \frac{1}{2i\omega}\int [r_\alpha j_\beta + r_\beta j_\alpha - \frac{2}{3}(\vec{r}\cdot\vec{j})\delta_{\alpha,\beta}]d^3r, \quad (8)$$

$$Q^{(m)}_{\alpha\beta} = \frac{1}{3c}\int [(\vec{r}\times\vec{j})_\alpha r_\beta + ((\vec{r}\times\vec{j})_\beta r_\alpha)]d^3r, \quad (9)$$

where c and ω are the speed and angular frequency of light, respectively, and $\alpha,\beta = x,y,z$. The $\vec{P}$, $\vec{M}$, $\vec{T}$, $\vec{Q}^{(e)}$, $\vec{Q}^{(m)}$ are electric dipole (ED) moment, magnetic dipole (MD) moment, toroidal dipole (TD) moment, electric quadrupole (EQ)

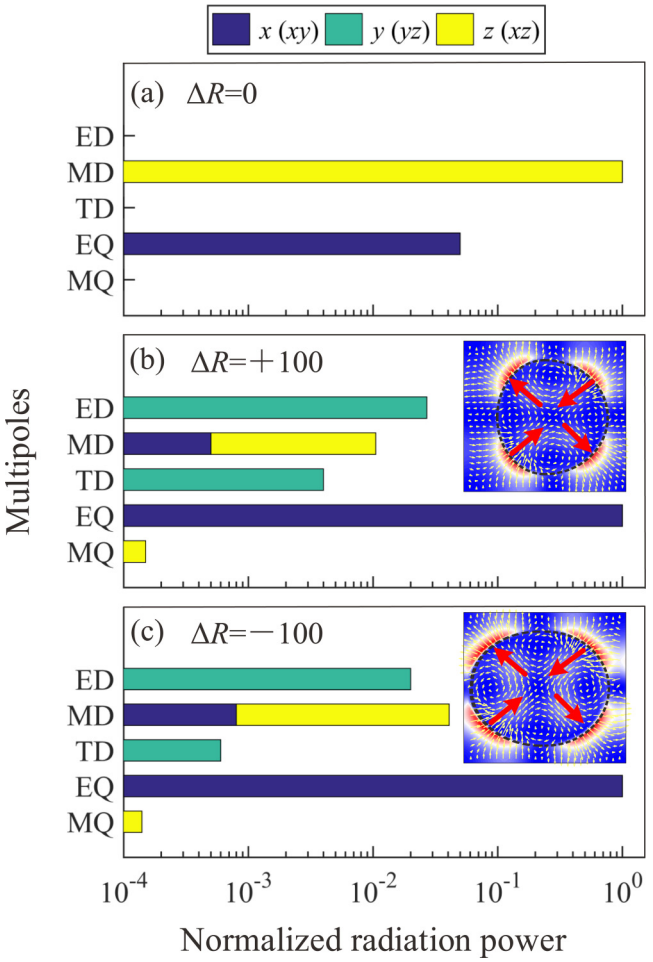

FIG. 3. The normalized radiation power of components of different multipoles for BIC (a) and quasi-BICs (b) and (c), where x, y, z components are considered for ED, MD, and TD, and xy, yz, xz components are considered for EQ and MQ. The electric field distributions are illustrated in the insets of (b) and (c), with yellow arrows representing the electric field vector and red arrows highlighting the directions.

moment, and magnetic quadrupole (MQ) moment, respectively. The scattered powers of these multipole moments are calculated from $I_P = \frac{2\omega^4}{3c^3}|\vec{P}|^2$, $I_M = \frac{2\omega^4}{3c^3}|\vec{M}|^2$, $I_T = \frac{2\omega^6}{3c^5}|\vec{T}|^2$, $I_{Q^{(e)}} = \frac{\omega^6}{5c^5}\sum|\vec{Q}^{(e)}_{\alpha\beta}|^2$, $I_{Q^{(m)}} = \frac{\omega^6}{40c^5}\sum|\vec{Q}^{(m)}_{\alpha\beta}|^2$. For BIC when $\Delta R = 0$, MD along the z axis contributes most. Another contributor is EQ in the x-y plane. Both these two multipole components do not radiate along the vertical z axis [6,53]. In addition, the radiation in the transverse plane is negligible owing to the array effect of the metasurface [6,38,44,54]. Therefore, BIC has zero radiation loss. After introduction of the symmetry perturbation, other multipole components possessing radiation along the z axis emerge, resulting in the excitation of quasi-BIC as illustrated in Figs. 3(b) and 3(c). Accompanying with the occurrence of sharp Fano resonances, the dominant multipole converts from MD to EQ, which originates from the uncompensated, opposite-oriented ED moments at the x-y plane in the two halves of the nanodisks with different areas as described in Fig. 2(b) [55]. This dominant EQ also manifests itself in the near-field distribution [the insets of Figs. 3(b) and 3(c)], illustrating two antiphase dipoles in the asymmetric nanodisk. These asymmetric dipoles also give rise to ED along the y axis, contributing to the emergence of Fano resonances as predicted in Eq. (4). As asymmetry degrees of the nanodisks grow, ED along the y axis radiates more strongly and degrades the light confinement ability of the nanodisks, which leads to resonances with broader linewidths and smaller Q factors as shown in Fig. 1(b). In addition, the x and z components of MD produce a circular magnetic field in the x-z plane, generating TD along the y axis accompanying with MQ in the x-z plane. It is also noted that the adding or removing operation evolves a specific BIC into quasi-BICs with similar near-field localization and far-field radiation, even if these quasi-BICs resonate at opposite sides of the BIC wavelength.

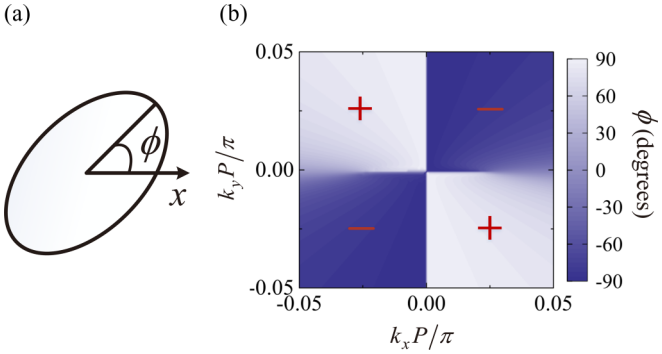

FIG. 4. (a) Sketch of the polarization angle ϕ in a polarization ellipse. (b) The polarization angle ϕ in the $\vec{k}$ space near the BIC. Red marks denote the signs of polarization angles.

III. TOPOLOGICAL NATURE

Finally, we demonstrate that this BIC is associated with vortices in the polarization field and evaluate its topological charge defined by the number of times the polarization vectors wind around the vortex center. The topological charge q carried by BIC is defined as [4,12,19,56]

$$q = \frac{1}{2\pi}\oint d\vec{k}\cdot\nabla_{\vec{k}}\phi(\vec{k}), \tag{10}$$

where the integration is performed in a closed path in $\vec{k}$ space that goes around the BIC in the counterclockwise direction, $\phi(\vec{k})$ is the angle of the polarization vector expressed as $\phi(\vec{k}) = \arg[E_x(\vec{k}) + iE_y(\vec{k})]$ [Fig. 4(a)]. Figure 4(b) illustrates the evolution of ϕ in $|\vec{k}| = 0.05\pi/P$, where $P = 1050$ nm is the period of unit cell. Performing Eq. (10) leads to $q = -1$. It is determined by the field eigenvalues of this C_4 rotational symmetry in the structure [56]. This topological nature of BIC guarantees its robust existence and governs its revolution.

IV. CONCLUSIONS

In summary, we study the properties of symmetry-protected BIC in highly symmetric nanodisks and demonstrate its transformation to quasi-BIC through removing or adding parts from the edge. A same inverse quadratic

dependence of Q_{rad} for quasi-BIC excited by these two opposite operations on the asymmetry degree is observed and explained in detail. Going deeper, contributions from different multipole components and distributions of electric field are calculated to explicate the evolutions from BIC to quasi-BIC and their characteristics. Finally, the topological characteristics of BIC are analyzed. This in-depth analysis of the symmetry-protected BIC and quasi-BIC supported by metasurfaces with single element and zero sharp corners in a unit cell may facilitate the realization of high Q-factor resonators with better performance.

ACKNOWLEDGMENTS

This work is supported by the National Natural Science Foundation of China (Grants No. 11847132 and No. 61901164), and Interdisciplinary Innovation Fund of Nanchang University (Grant No. 2019-9166-27060003).

[1] C. W. Hsu, B. Zhen, A. D. Stone, J. D. Joannopoulos, and M. Soljačić, Nat. Rev. Mater. **1**, 16048 (2016).
[2] K. Koshelev, G. Favraud, A. Bogdanov, Y. Kivshar, and A. Fratalocchi, Nanophotonics **8**, 725 (2019).
[3] J. von Neumann and E. Wigner, Phys. Z. **30**, 465 (1929).
[4] K. Koshelev, S. Lepeshov, M. Liu, A. Bogdanov, and Y. Kivshar, Phys. Rev. Lett. **121**, 193903 (2018).
[5] A. C. Overvig, S. C. Malek, M. J. Carter, S. Shrestha, and N. Yu, arXiv:1903.11125.
[6] Z. Sadrieva, K. Frizyuk, M. Petrov, Y. Kivshar, and A. Bogdanov, Phys. Rev. B **100**, 115303 (2019).
[7] Z. F. Sadrieva, M. A. Belyakov, M. A. Balezin, P. V. Kapitanova, E. A. Nenasheva, A. F. Sadreev, and A. A. Bogdanov, Phys. Rev. A **99**, 053804 (2019).
[8] A. S. Kupriianov, Y. Xu, A. Sayanskiy, V. Dmitriev, Y. S. Kivshar, and V. R. Tuz, Phys. Rev. Appl. **12**, 014024 (2019).
[9] C. W. Hsu, B. Zhen, J. Lee, S.-L. Chua, S. G. Johnson, J. D. Joannopoulos, and M. Soljačić, Nature (London) **499**, 188 (2013).
[10] M. V. Rybin, K. L. Koshelev, Z. F. Sadrieva, K. B. Samusev, A. A. Bogdanov, M. F. Limonov, and Y. S. Kivshar, Phys. Rev. Lett. **119**, 243901 (2017).
[11] A. A. Bogdanov, K. L. Koshelev, P. V. Kapitanova, M. V. Rybin, S. A. Gladyshev, Z. F. Sadrieva, K. B. Samusev, Y. S. Kivshar, and M. F. Limonov, Adv. Photonics **1**, 016001 (2019).
[12] H. M. Doeleman, F. Monticone, W. den Hollander, A. Alù, and A. F. Koenderink, Nat. Photonics **12**, 397 (2018).
[13] K. L. Koshelev, S. K. Sychev, Z. F. Sadrieva, A. A. Bogdanov, and I. V. Iorsh, Phys. Rev. B **98**, 161113(R) (2018).
[14] T. Lepetit and B. Kanté, Phys. Rev. B **90**, 241103(R) (2014).
[15] V. Mocella and S. Romano, Phys. Rev. B **92**, 155117 (2015).
[16] J. Jin, X. Yin, L. Ni, M. Soljačić, B. Zhen, and C. Peng, Nature (London) **574**, 501 (2019).
[17] Y. Plotnik, O. Peleg, F. Dreisow, M. Heinrich, S. Nolte, A. Szameit, and M. Segev, Phys. Rev. Lett. **107**, 183901 (2011).
[18] L. S. Li, J. Zhang, C. Wang, N. Zheng, and H. Yin, Phys. Rev. A **96**, 013801 (2017).
[19] E. N. Bulgakov and D. N. Maksimov, Phys. Rev. A **96**, 063833 (2017).
[20] Y. He, G. Guo, T. Feng, Y. Xu, and A. E. Miroshnichenko, Phys. Rev. B **98**, 161112(R) (2018).
[21] A. Kodigala, T. Lepetit, Q. Gu, B. Bahari, Y. Fainman, and B. Kanté, Nature (London) **541**, 196 (2017).
[22] S. T. Ha, Y. H. Fu, N. K. Emani, Z. Pan, R. M. Bakker, R. Paniagua-Domínguez, and A. I. Kuznetsov, Nat. Nanotechnol. **13**, 1042 (2018).
[23] S. Romano, G. Zito, S. Torino, G. Calafiore, E. Penzo, G. Coppola, S. Cabrini, I. Rendina, and V. Mocella, Photonics Res. **6**, 726 (2018).
[24] K. Koshelev, Y. Tang, K. Li, D.-Y. Choi, G. Li, and Y. Kivshar, ACS Photonics **6**, 1639 (2019).
[25] L. Xu, K. Zangeneh Kamali, L. Huang, M. Rahmani, A. Smirnov, R. Camacho-Morales, Y. Ma, G. Zhang, M. Woolley, D. Neshev, and A. E. Miroshnichenko, Adv. Sci. **6**, 1802119 (2019).
[26] L. Carletti, S. S. Kruk, A. A. Bogdanov, C. De Angelis, and Y. Kivshar, Phys. Rev. Res. **1**, 023016 (2019).
[27] S. D. Krasikov, A. A. Bogdanov, and I. V. Iorsh, Phys. Rev. B **97**, 224309 (2018).
[28] K. Koshelev, A. Bogdanov, and Y. Kivshar, Sci. Bull. **64**, 836 (2018).
[29] A. Tittl, A. Leitis, M. Liu, F. Yesilkoy, D.-Y. Choi, D. N. Neshev, Y. S. Kivshar, and H. Altug, Science **360**, 1105 (2018).
[30] M. Liu, D. A. Powell, R. Guo, I. V. Shadrivov, and Y. S. Kivshar, Adv. Opt. Mater. **5**, 1600760 (2017).
[31] F. Yesilkoy, E. R. Arvelo, Y. Jahani, M. Liu, A. Tittl, V. Cevher, Y. Kivshar, and H. Altug, Nat. Photonics **13**, 390 (2019).
[32] V. A. Fedotov, M. Rose, S. L. Prosvirnin, N. Papasimakis, and N. I. Zheludev, Phys. Rev. Lett. **99**, 147401 (2007).
[33] V. V. Khardikov, E. O. Iarko, and S. L. Prosvirnin, J. Optics **12**, 045102 (2010).
[34] R. Singh, I. A. Al-Naib, Y. Yang, D. Roy Chowdhury, W. Cao, C. Rockstuhl, T. Ozaki, R. Morandotti, and W. Zhang, Appl. Phys. Lett. **99**, 201107 (2011).
[35] A. B. Evlyukhin, S. I. Bozhevolnyi, A. Pors, M. G. Nielsen, I. P. Radko, M. Willatzen, and O. Albrektsen, Nano Lett. **10**, 4571 (2010).
[36] F. Zhang, X. Huang, Q. Zhao, L. Chen, Y. Wang, Q. Li, X. He, C. Li, and K. Chen, Appl. Phys. Lett. **105**, 172901 (2014).
[37] W. X. Lim and R. Singh, Nano Converg. **5**, 5 (2018).
[38] S. Campione, S. Liu, L. I. Basilio, L. K. Warne, W. L. Langston, T. S. Luk, J. R. Wendt, J. L. Reno, G. A. Keeler, I. Brener, and M. B. Sinclair, ACS Photonics **3**, 2362 (2016).
[39] P. P. Vabishchevich, S. Liu, M. B. Sinclair, G. A. Keeler, G. M. Peake, and I. Brener, ACS Photonics **5**, 1685 (2018).
[40] Z. F. Sadrieva, I. S. Sinev, K. L. Koshelev, A. Samusev, I. V. Iorsh, O. Takayama, R. Malureanu, A. A. Bogdanov, and A. V. Lavrinenko, ACS Photonics **4**, 723 (2017).
[41] V. R. Tuz, V. V. Khardikov, A. S. Kupriianov, K. L. Domina, S. Xu, H. Wang, and H.-B. Sun, Opt. Express **26**, 2905 (2018).

[42] E. D. Palik, *Handbook of Optical Constants of Solids*, Vol. 3 (Academic Press, Cambridge, 1998).
[43] C. Wu, N. Arju, G. Kelp, J. A. Fan, J. Dominguez, E. Gonzales, E. Tutuc, I. Brener, and G. Shvets, Nat. Commun. **5**, 3892 (2014).
[44] Y. Yang, I. I. Kravchenko, D. P. Briggs, and J. Valentine, Nat. Commun. **5**, 5753 (2014).
[45] L. Huang, Y. Yu, and L. Cao, Nano Lett. **13**, 3559 (2013).
[46] P. Yu, A. S. Kupriianov, V. Dmitriev, and V. R. Tuz, J. Appl. Phys. **125**, 143101 (2019).
[47] J. M. Foley, S. M. Young, and J. D. Phillips, Phys. Rev. B **89**, 165111 (2014).
[48] M. B. Doost, W. Langbein, and E. A. Muljarov, Phys. Rev. A **90**, 013834 (2014).
[49] A. B. Evlyukhin, T. Fischer, C. Reinhardt, and B. N. Chichkov, Phys. Rev. B **94**, 205434 (2016).
[50] Y. Fan, F. Zhang, N.-H. Shen, Q. Fu, Z. Wei, H. Li, and C. M. Soukoulis, Phys. Rev. A **97**, 033816 (2018).
[51] P. C. Wu, C. Y. Liao, V. Savinov, T. L. Chung, W. T. Chen, Y.-W. Huang, P. R. Wu, Y.-H. Chen, A.-Q. Liu, N. I. Zheludev, and D. P. Tsai, ACS Nano **12**, 1920 (2018).
[52] W. X. Lim, S. Han, M. Gupta, K. F. MacDonald, and R. Singh, Appl. Phys. Lett. **111**, 061104 (2017).
[53] W. Chen, Y. Chen, and W. Liu, Phys. Rev. Lett. **122**, 153907 (2019).
[54] V. A. Fedotov, N. Papasimakis, E. Plum, A. Bitzer, M. Walther, P. Kuo, D. P. Tsai, and N. I. Zheludev, Phys. Rev. Lett. **104**, 223901 (2010).
[55] V. R. Tuz, V. V. Khardikov, and Y. S. Kivshar, ACS Photonics **5**, 1871 (2018).
[56] B. Zhen, C. W. Hsu, L. Lu, A. D. Stone, and M. Soljačić, Phys. Rev. Lett. **113**, 257401 (2014).